Cavity-resonator integrated bi-atom grating coupler for enhanced second-harmonic generation

Anne-Laure Fehrembach, Evgueni Popov, Elizabeth Hemsley, Antoine Monmayrant, Olivier Gauthier-Lafaye, Stéphane Calvez

Research Article | Vol. 30, No. 21 / 10 Oct 2022 / Optics Express 38789

Optics EXPRESS

Cavity-resonator integrated bi-atom grating coupler for enhanced second-harmonic generation

ANNE-LAURE FEHREMBACH,[1,*] EVGUENI POPOV,[1,2] ELIZABETH HEMSLEY,[1,3] ANTOINE MONMAYRANT,[3] OLIVIER GAUTHIER-LAFAYE,[3] AND STÉPHANE CALVEZ[3]

[1]Aix Marseille Univ., CNRS, Centrale Marseille, Institut Fresnel, Marseille, France
[2]Institut Universitaire de France, France
[3]LAAS-CNRS, Université de Toulouse, CNRS, 7 Avenue du Colonel Roche, F-31400 Toulouse, France
[*]anne-laure.fehrembach@fresnel.fr

Abstract: We report on the design of cavity-resonator integrated grating couplers for second-harmonic generation. The key point is that the base pattern of our grating coupler (GC) is made of two ridges with different widths (bi-atom). Thus, we reach extremely high Q-factors (above 10^5) with structures whose fabrication is not challenging, since the bi-atom base pattern is close to that of the surrounded distributed Bragg reflectors (DBR). Yet, the parameters of the structure have to be chosen cautiously to reduce the transition losses between each section (GC, DBR). We numerically demonstrate conversion efficiencies η of several tenths per Watt, even doubled when we include a phase-matching grating within the structuration. Such efficiencies are comparable to those obtained with waveguides and nano-resonators.

1. Introduction

Non-linear optics is a very active field of research in which the exploitation of nanotechnologies has played a prevalent role for about fifteen years. The objective is to overcome the difficulties related to very low non-linear susceptibilities.

In a previous publication, we have demonstrated the potential for second harmonic generation (SHG) of a structure called a CRIGF, a cavity-resonator integrated filter [1]. CRIGF are composed from a grating coupler (GC), surrounded by two distributed Bragg reflectors (DBRs), the distance between them being tunable thanks to a phase section (PS) (see Fig. 1 (a)). On the one hand, the CRIGF appears as an alternative solution, in a context of miniaturisation of the components, to ribbon and slab waveguides, in which high conversion rates are reached thanks to ingenious designs aim to fulfil the phase matching condition between the pump and signal waves [2–9]. On the other hand, the CRIGFs present macroscopic scale modal volumes, whereas the high conversion rates in nano-resonators rely on the excitation of modes with wavelength scale modal volumes and long lifetime for which the interaction time with the non-linear material is increased [10–14]. Thanks to this difference in the scales, we can expect the non-linear conversion to be much less sensitive to manufacturing defects in CRIGFs than in nano-resonators. Hence, the CRIGF appear as a promising intermediate solution, in term of scale, between waveguides and nano-resonators. Moreover, the mode of a CRIGF is efficiently excited with a few-wavelengths-diameter free space incident beam, which is easily achieved with conventional optics. As compared to the classical guided-mode resonance gratings, which require highly collimated beams, the CRIGFs thus allow greater enhancement of the pump field density [1].

For our first attempt at SHG in a CRIGF [1], we demonstrated numerically a conversion ratio $\eta = 8.2 \times 10^{-6}\,\mathrm{W}^{-1}$ and experimentally $1.9 \times 10^{-6}\,\mathrm{W}^{-1}$. The SHG conversion ratio is defined as $\eta = P_{2\omega}/[P_\omega]^2$, where P_ω is the power of the pump beam at frequency ω, and $P_{2\omega}$ is the total

#468683 https://doi.org/10.1364/OE.468683
Journal © 2022 Received 23 Jun 2022; revised 21 Sep 2022; accepted 22 Sep 2022; published 5 Oct 2022

Optics EXPRESS

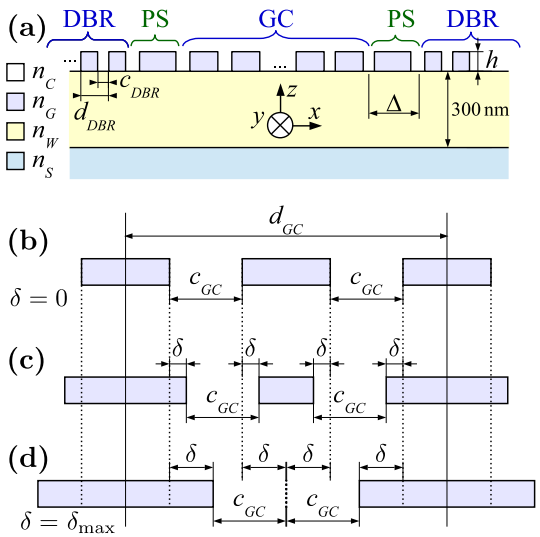

Fig. 1. Description of the structure: CRIGF (a) with grating coupler (GC, N_{GC} periods), surrounded with a phase section (PS, width Δ taken between the centers of the adjacent grooves) and distributed Bragg reflectors (DBR, N_{DBR} periods each side) with period d_{DBR} and holes width c_{DBR}; "bi-atom" pattern with constant hole width c_{GC} and increasing perturbation $\delta = 0$ (b), $\delta \neq 0$ (c) and $\delta = \delta_{\max}$.

power emitted at the signal frequency 2ω. This result has been obtained without optimization of the parameters aimed at enhancing the SHG: the component was only designed to exhibit a sharp resonance peak in its reflectivity spectrum at the pump frequency.

Two methods to enhance the SHG are possible. Firstly, the component has to be resonant for both the pump and the signal frequencies, and designed to ensure a good overlap between the modes within the non-linear material, together with a phase matching between the two modes so that the waves generated by the non-linear process interfere constructively. In the case of CRIGF, this means one guided mode at ω and another at 2ω with the same effective index. This can be obtained either using an adequate orientation of the anisotropic Lithium Niobate crystal, or a more complex layer stack.

The second method is to enhance the quality factor Q of the resonance at the signal frequency, and thus the pump field inside the component. The Q-factor is defined as the ratio of the resonance wavelength λ to the spectral full width at half maximum $\Delta\lambda$ of the emitted power: $Q = \lambda/\Delta\lambda$. The resonances in a CRIGF are Fabry-Perot resonances of guided modes, that leak through the GC region. Hence, the Q-factor of a CRIGF resonance is related to both the quality factor of the Fabry-Perot resonator and to the quality factor of the GC.

The DBRs are usually chosen long enough to ensure negligible transmission losses, and we know that the quality factor of the Fabry-Perot resonator can be tuned linearly with the length of the cavity. A more interesting path is to enhance the Q-factor of the GC, e.g. decrease the losses through the GC, as several parameters can be used to adjust its response. Indeed, the strength of the in and out coupling in a guided mode resonant grating depends quadratically on three quantities: (1) the grating depth, (2) the overlap integral between the eigenmode and the free space waves, and (3) the modulus of the Fourier coefficient of the grating permittivity function associated with the in/out coupling diffraction order (first one in most cases) [15]. Reducing the GC depth will lead to a small DBRs depth, thus inefficient DBRs, as both GC and DBRs are usually etched in one single fabrication step. A more promising idea is to tune down the overlap

Optics EXPRESS

integral by moving the GC sideways using non-symmetric PS sections and thus breaking the symmetry of the CRIGF. This is described in our recent paper [16], and can lead to conversion ratio greater than $4.3 \times 10^{-3}\,\mathrm{W}^{-1}$.

Finally, the first Fourier coefficient of the GC permittivity function can be made extremely small thanks to a suitable base pattern. A naive approach is to consider a GC with an extremely low (or extremely high) filling factor, but it is experimentally extremely challenging as it requires the fabrication of few-nanometers-wide grooves (or bumps) with high aspect ratio. A more promising approach is the so-called "bi-atom" base pattern, composed of two bumps (for gratings periodic along one direction) with different widths [17,18].

In the present work, we explore the ways to design a CRIGF with a bi-atom base pattern for the GC, and quantify the SHG conversion ratio that can be expected considering the possibilities of the present manufacturing process. The second section introduces the notations and the overall designs rules. The third and fourth sections present two different ways of optimizing the bi-atom CRIGFs to enhance the SHG. In the fifth section, further improvements are made using grating phase-matching.

2. Notations and overall design rules

As in [16], the stack depicted in Fig. 1 (a) is composed of a 300 nm-thick layer of $LiNbO_3$ (index n_W), deposited on a SiO_2 substrate (index n_S). A pattern of depth h is engraved on a Si_3N_4 layer (index n_G). The cover is air (index n_C).

The pump wavelength is set at $\lambda_0 = 1.55\,\mu$m. The values of the index at the pump frequency ω are: $n_S = 1.444$, $n_W = 2.1316$, $n_G = 1.9963$ and $n_C = 1.0$. At the signal frequency 2ω they are $n_S = 1.4538$, $n_W = 2.1793$, $n_G = 2.0259$ and $n_C = 1.0$. The pattern is composed of a grating coupler (GC) with $N_{GC} = 21$ periods, surrounded by Distributed Bragg Reflectors (DBR), with N_{DBR} periods. For each structure, N_{DBR} is chosen the ensure that the losses through the DBR at the edges of the structure are negligible. The remaining parameters of the structure are chosen following the rules described below, aimed at maximizing the pump field in the structure.

The pattern depth h is the result of a trade-off. On the one hand, when h decreases, the radiation losses caused by the GC also decrease and the Q-factor increases. Yet, as we plan to fabricate the component with e-beam lithography followed by RIE etching, the depth of the DBR must be the same as that of the GC. And on the other hand, the reflectivity of the DBR follows the variations of h, and small h means long DBR. Hence, we chose $h = 50$ nm for which $N_{DBR} = 400$ periods for the DBR are generally sufficient to obtain less than 0.1 % transmission losses through the DBR.

To choose the periods and the holes width of the DBR and GC, we have to go deeper into the understanding of the CRIGF. The CRIGF is first of all a Fabry-Perot cavity [19,20]. The resonances are Fabry-Perot resonances of the modes that are inside the gap of the DBR. Thus, their effective index $\tilde{n}$ and resonance wavelength $\tilde{\lambda}$ satisfy

$$\frac{2\pi}{\tilde{\lambda}}\tilde{n} = \frac{\pi}{d_{DBR}}, \tag{1}$$

where d_{DBR} is the period of the DBR and

$$\frac{2\pi}{\tilde{\lambda}}\tilde{n}L_{eff} = p\pi, \tag{2}$$

where L_{eff} is the effective length of the cavity, including the penetration depth of the field inside the DBR, and p is a natural integer.

Second, the GC is here to couple in/out this mode. The in/out coupling will be resonant if the wavelength and effective index of the Fabry-Perot cavity mode matches those of a mode of the GC, more precisely if $(\tilde{n}, \tilde{\lambda})$ is close to a point of the dispersion relation of the GC. As we

Optics EXPRESS

intend to have a resonant in/out coupling of the Fabry-Perot mode in normal incidence through the first diffraction order of the GC, this means that $(\tilde{n}, \tilde{\lambda})$ must correspond to one of the edge of the second order band gap of the GC, preferably the symmetric mode edge. In this case, the required condition is

$$\frac{2\pi}{\tilde{\lambda}}\tilde{n} = \frac{2\pi}{d_{GC}} \tag{3}$$

where d_{GC} is the period of the GC and $\tilde{\lambda}$ is close to the wavelength of the symmetric-mode band edge of the GC. We could choose the anti-symmetric-mode band edge, not coupled with free-space waves for an infinite GC, and leading to a very high Q mode for the finite GC included in the CRIGF. We could also choose a coupling in/out under oblique incidence [21]. These two developments may be interesting but are out of the scope of this paper.

The Eqs. (1) and (3) set the relation between the periods of the DBR and GC

$$d_{GC} = 2d_{DBR}, \tag{4}$$

and ensure that the propagation constant $(2\pi/\tilde{\lambda})\tilde{n}$ of the mode excited at the band edge of the GC is equal to those of the modes inside the band gap of the DBRs. Hence the optimization procedure aims at matching the wavelengths of the GC mode and that of the Fabry-Perot mode (within a range set by the DBRs band gap).

The GC considered here is a bi-atom base pattern grating, depicted in Fig. 1 (c), composed of two holes with same width c_{GC}, and two bumps, one large with width $d_{GC}/2 - c_{GC} + 2\delta$, and one small with width $d_{GC}/2 - c_{GC} - 2\delta$. As a reference, the pattern for $\delta = 0$ (bumps with equal widths) is represented in Fig. 1 (b). The range of variation of c_{GC} is $[0; d_{GC}/2 - 2\delta]$, and the range for δ is $[0; \delta_{\max} = d_{GC}/4 - c_{GC}/2]$, the upper boundary corresponding to the vanishing of the small bump, as shown in Fig. 1 (d).

The Q-factor of the GC scales like $1/|\epsilon_1|^2$, where ϵ_1 is the first Fourier coefficient of the grating pattern. The latter is given by

$$|\epsilon_1|^2 = \left[(2/\pi)(n_G^2 - n_C^2)\sin(2\pi\delta/d_{GC})\sin(\pi c_{GC}/d_{GC})\right]^2. \tag{5}$$

As expected, ϵ_1 is null for $\delta = 0$, and increases with δ for values of δ smaller than $d_{GC}/4$. It also increases with c_{GC} in its range of variation. We can thus achieve extremely high Q-factors for the GC for δ close to 0, that is for GC patterns resembling the side DBRs of the CRIGF. These patterns are thus not particularly challenging to fabricate.

The width of the gap of the GC depends on the modulus of the second Fourier coefficient of the pattern [15], given by

$$|\epsilon_2| = \left|(1/\pi)(n_G^2 - n_C^2)\cos(4\pi\delta/d_{GC})\sin(2\pi c_{GC}/d_{GC})\right|. \tag{6}$$

It is maximum for $\delta = 0$, and $c_{GC} = d_{GC}/4$. For lossless materials, ϵ_2 is real and a change in its sign means an exchange of the respective position of the symmetric and anti-symmetric modes on the upper or lower edges of the band gap. The bi-atom pattern as described here leads to a symmetric mode at a greater wavelength than the anti-symmetric mode for values of δ smaller than $d_{GC}/8$. The opposite can be obtained with the complementary pattern obtained by swapping the air grooves and the high-index bumps.

At this point, the reader can understand that the bi-atom pattern GC with δ close to 0 and $c_{GC} = d_{GC}/4$ has a spectral band gap very close to that of a DBR with period $d_{DBR} = d_{GC}/2$ and a 1/2 filling factor (for which the DBR band gap width is maximum). Hence, such parameters lead to a GC mode wavelength too close to one edge of the DBR band gap, resulting in inefficient Bragg reflections.

As a consequence, as a *first step* of our optimization scheme, the infinite GC and DBR are modelled, and their dispersion relation are calculated with respect to their parameters. We

Optics EXPRESS

optimize both GC and DBR parameters to bring the symmetric-mode wavelength of the GC at the design wavelength $\lambda_0 = 1.55\,\mu$m and inside the DBR band gap. There is an infinity of possibilities to realize this adjustment, and we will explore two ways in the two next sections.

The *second step* is to determine the PS length Δ, defined as the distance between the centers of the GC last groove and DBR first groove (see Fig. 1 (a)). To do so, the whole CRIGF is modelled, and Δ is chosen so that the field amplitude is maximum for the wavelength λ_0. More precisely, we calculate the field amplitude at the bottom of the $LiNbO_3$ guiding layer at the center of the structure along x. It would be more accurate, to optimize the SHG signal, to maximize the integral of the square modulus of the electric field inside the $LiNbO_3$ layer, but at the cost of much longer calculations that the gain in precision does not justify. The *third step* is to calculate the SHG emitted power in the substrate and the superstrate.

Throughout the paper, the calculations are made with a home-made numerical code based on the Fourier Modal Method. The finite size of the CRIGF along x is taken into account by applying the so called "super-cell" technique [22], and both the structure and the incident Gaussian beam are invariant along y (2D structure and 2D beam). The electric field is along y (s polarization). The SHG calculations are done with the same code, under the undepleted pump approximation [23,24]. We have validated our Fourier Modal Method code by comparison with another of our home-made numerical code based on the Finite Element Method.

From the SHG emitted power we calculate the conversion efficiency factor $\eta = P_{2\omega}/[P_\omega]^2$. In order to be able to compare our calculations with the real case of a 3D Gaussian beam, η is estimated by taking into account a correction factor, as explained in [16].

3. CRIGF with an optimized bi-atom GC and 0.5-filling-factor DBRs

At a first sight, its seems natural to work with an optimized DBR, e.g. a DBR with a filling factor $ff_{DBR} = 0.5$, and a wavelength in the middle of its band gap.

Hence, in this part, $ff_{DBR} = c_{DBR}/d_{DBR} = 1/2$, giving a guided mode with effective index $\tilde{n} = 1.759$, and we choose a period $d_{DBR} = 440.6\,$nm to center the gap of the DBR at $\lambda_0 = 1.55\,\mu$m. The imaginary part of the propagation constant of the mode in the DBR at λ_0 is $0.058\,\mu\text{m}^{-1}$, for which $N_{DBR} = 400$ is sufficient to ensure a quasi-total reflection.

In order to change the Q-factor of the GC, we vary the value of δ from 2.5 nm to 20 nm. For $c_{GC} = d_{GC}/4$, the guided mode in the GC has the same effective index as in the DBR, leading to a GC gap centered at $1.55\,\mu$m. For the bi-atom pattern describe in Fig. 1 (c), as the symmetric mode is at greater wavelengths, we must increase the hole width c_{CG} to bring it down to λ_0. The calculations are done modelling the infinite GC. We plot in Fig. 2 the evolution of the wavelength for symmetric (blue line) anti-symmetric (orange line) modes with respect to c_{GC}/d_{GC} for $\delta = 20\,$nm. The grey area represents the DBR band gap and the green line represents the design wavelength $\lambda_0 = 1.55\,\mu$m. As expected for this structure, we observe that the symmetric mode is at a larger wavelength than the anti-symmetric one, and that the GC band gap moves to lower wavelengths as c_{GC} increases. It is close to the DBR band gap for $c_{GC}/d_{GC} = 1/4$.

From this plot, we choose the value of c_{GC} that puts the symmetric mode at λ_0, in the middle of the DBR gap, $c_{GC}/d_{GC} \simeq 0.36$ (dashed line in Fig. 2). We proceed in the same manner for the other values of δ. The corresponding values of c_{GC} are given in Table 1.

The entire CRIGF is then modelled to determine the size of the PS maximizing the field amplitude. We choose two consecutive values of Δ among the d_{DBR}-periodic values of Δ for which the Fabry-Perot resonances occur at λ_0, leading to two sets of structures, labelled "a" and "b" (see Table 1). The PS in the set "b" is around $\lambda_0/(2\tilde{n})$ greater than the PS in set "a".

We plot in Fig. 3 the field amplitude (normalized with respect to the square root of the incident power) versus the Q-factor of the CRIGF resonance (calculated from the spectral dependence of field amplitude) for each structure (blue for set "a", and orange for set "b"). The labels correspond to the structures listed in Table 1. Considering each set of results, given on the one

Optics EXPRESS

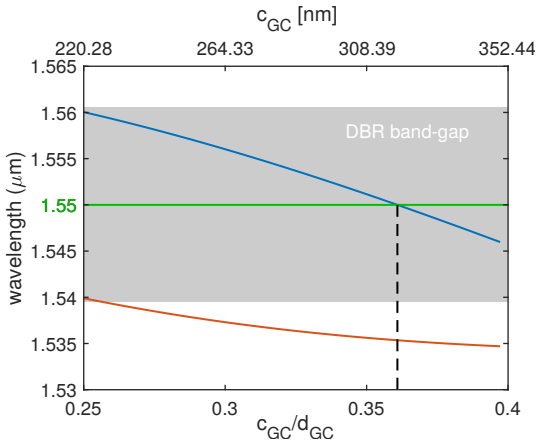

Fig. 2. Wavelength of the symmetric (blue line) and anti-symmetric (orange line) modes with respect to c_{GC}/d_{GC} for the GC with $\delta = 20$ nm, $d_{GC} = 881.1$ nm. The DBR band gap is represented in grey, and the design wavelength λ_0 in green.

Table 1. Parameters of the CRIGF with an optimized bi-atom GC and DBR filling factor[a]

Structure	δ	c_{GC}	Δ
GC2.5a	2.5	320.5	335.3
GC5a	5	320.4	337.8
GC10a	10	320.0	342.9
GC15a	15	319.2	347.9
GC20a	20	318.0	352.9
GC2.5b	2.5	320.5	770.5
GC5b	5	320.4	773.0
GC10b	10	320.0	778.1
GC15b	15	319.2	783.1
GC20b	20	318.0	788.0

[a]$ff_{DBR} = 0.5$, all dimensions in nanometers. Common parameters: $d_{DBR} = 440.6$ nm, $c_{DBR} = 220.3$ nm, $N_{DBR} = 400$, $d_{GC} = 881.2$ nm, $N_{GC} = 21$.

Optics EXPRESS

hand for the smaller values of Δ, and on the other hand for the greater values, we can see that the Q-factor increases when δ decreases, as expected. The Q-factors for the set "b" are larger than for set "a", thanks to longer Fabry-Perot cavities. We can also observe that the field amplitude reaches a maximum when the Q factor increases (for $\delta = 10\,\text{nm}$ for the set "a" and $\delta = 5\,\text{nm}$ for the set "b"), and then decreases for greater Q factors. This phenomenon has already been observed for other kind of resonators [25,26], and most recently for CRIGF [27]. The maximum of the field amplitude is related to a balance, known as critical coupling, between (useful) in/out coupling losses through the GC, and (unwanted) scattering losses coming from the mismatch between the modes in the successive regions (GC, PS and DBR). As already suggested in [16], the scattering losses can be reduced, and the maximum of the field amplitude increased, by introducing an additional groove within the phase section PS. We will perform this improvement on the structures studied in the following paragraph.

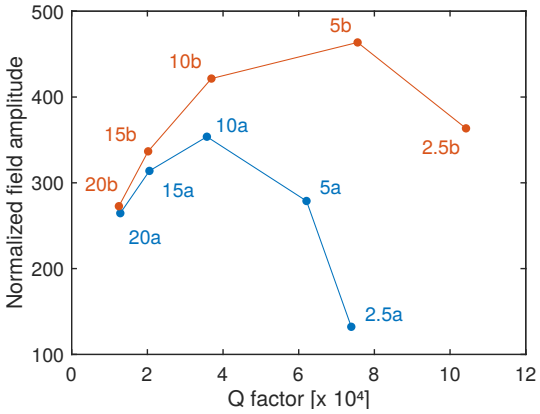

Fig. 3. Mode amplitude, normalized with respect to the square root of the incident power ($\text{V}.\mu\text{m}^{-1}.\text{W}^{-1/2}$), versus the Q-factor for the CRIGF of Table 1 (blue for set a, and orange for set b).

Finally, we plot in Fig. 4 the SHG conversion ratio η with respect to the fourth power of the normalized field amplitude. As expected, the greater the field amplitude, the greater the SHG conversion ratio. Moreover, the values show a linear dependence of $\log(\eta)$ with respect to the logarithm of the fourth power of the field amplitude, with a slope close to unity, confirming the fact that the SHG is mainly governed by the field amplitude and that the overlap integral between the field mode squared within the non-linear material stay almost constant for all the structures of Table 1.

The greater conversion ratio for these structures is $\eta = 3.5 \times 10^{-3}\,\text{W}^{-1}$ (for structure GC5b), which is of the same order of magnitude than with the non symmetric CRIGFs ($4.3 \times 10^{-3}\,\text{W}^{-1}$) proposed in [16].

Note that by increasing c_{GC}, we increased the factor growth of $|\epsilon_1|^2$ with respect to δ (see Eq. (5)), and thus decrease the Q-factor of the GC. Greater Q-factors can be obtained with smaller c_{GC} values, but requires the adjustment of the filling factor of the DBR to center the wavelength of the symmetric edge of the GC in the middle of the DBR gap. This is done in the following section.

Optics EXPRESS

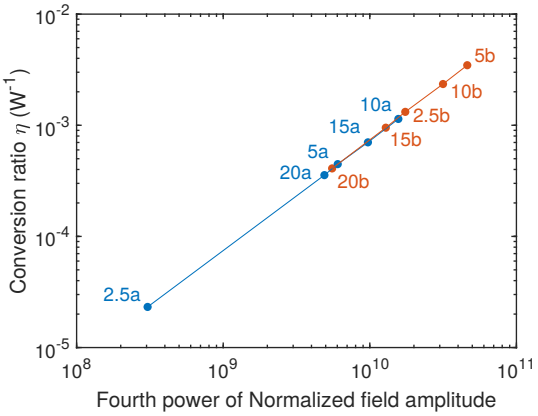

Fig. 4. SHG conversion ratio, with respect to the fourth power of the normalized field amplitude ([V.μm^{-1}.W$^{-1/2}$]^4) for the CRIGF of Table 1 (blue for set a, orange for set b).

4. CRIGF with an optimized bi-atom GC and DBR

In this section, we explore a second way to bring the symmetric-mode wavelength of the GC inside the DBR band gap, trying to keep a GC with a large Q-factor. Hence, we choose a GC such that $c_{GC}/d_{GC} = 0.257$, which will lead to smaller $|\epsilon_1|^2$ and thus greater Q-factor of the GC than for structures of section 2. This GC thus have a filling factor in groove of $ff_{GC} = 2c_{GC}/d_{GC} = 0.514$. The effective index of the fundamental TE guided mode is $\tilde{n} = 1.771$. The period of the DBR and GC adapted for this mode are $d_{DBR} = 437.2$ nm, and $d_{GC} = 874.4$ nm, leading to $c_{GC} = 225$ nm.

To choose the hole width of the DBR, we analyse its impact on the band gap of the DBR. We plot in Fig. 5 (a) the band gap of the DBR (gray area) and its central wavelength (black line) with respect to ff_{DBR}. We observe that it is shifted towards lower wavelengths as ff_{DBR} increases, and that its width decreases as ff_{DBR} moves away from 0.5. From this plot, we deduce that ff_{DBR} must be smaller than 0.5 to keep the design wavelength $\lambda_0 = 1.55$ μm (green line in Fig. 5 (a)) within the DBR band gap. We also plot, in Fig. 5 (b), the imaginary part of the propagation constant of the mode γ with respect to ff_{DBR}, in black for the wavelength at the center of the band gap (different for each value of ff_{DBR}) and in green at the design wavelength $\lambda_0 = 1.55$ μm. For the wavelength at the center of the band gap, Im(γ) increases with the band gap width. And for a given value of ff_{DBR}, Im(γ) is maximum at the center of the band gap. From this plot, we choose $ff_{DBR} = 0.366$ (black dashed line in Fig. 5), corresponding to $c_{DBR} = 160$ nm, for which the imaginary part of the propagation constant of the mode is almost maximum. It is equal to 0.046 μm^{-1}, 20 % smaller than for the mode in the middle of the band gap for which Im(γ) = 0.058 μm^{-1} (see Fig. 5 (b), black curve). Nevertheless, a DBR with $N_{DBR} = 400$ will be sufficient to ensure a quasi-total reflection of the mode by the DBR.

Next, the whole CRIGF is numerically modelled to determine the length Δ of the PS needed to center the resonance at 1.55 μm. The parameters for structures DBR1.25, DBR2.5, DBR5 and DBR10 with δ from 1.25 nm to 10 nm are gathered in Table 2.

We plot in Fig. 6 the value of the field amplitude (normalized with respect to the square root of the incident power) versus the Q-factor of the CRIGF resonance for theses structures (blue dots). We observe much greater Q-factors and field amplitudes than for the structures of section 2. This is in part due to the greater Q-factor of the GC, and also to the greater effective length of the cavity for the structures of section 3, as the DBR is less reflective. We still observe the same decrease of the field amplitude after an optimal Q-factor, due to the mode mismatch between the successive GC, PS and DBR regions. Yet, the mismatch may be smaller for the structures of

Optics EXPRESS

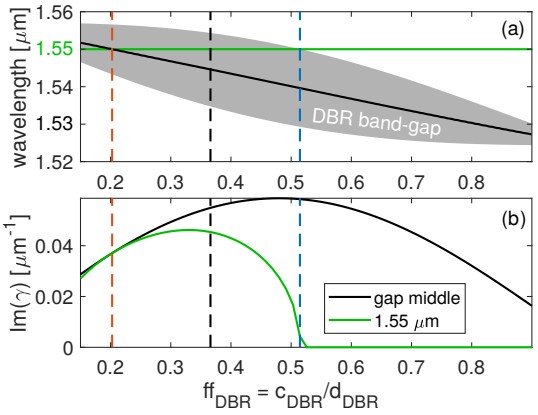

Fig. 5. Evolution with the filling factor of the DBR ff_{DBR} of (a) the DBR band-gap (grey area) and its central wavelength (black) and (b) the imaginary part of the propagation constant at the central wavelength of the band gap (black) and at the design wavelength (green).

Table 2. Parameters of the CRIGF with an optimized bi-atom GC and DBR[a]

Structure	δ	Δ
DBR1.25	1.25	806.4
DBR2.5	2.5	807.7
DBR5	5	810.0
DBR10	10	815.6

[a]All dimensions in nanometers. Common parameters: d_{DBR} = 437.2 nm, c_{DBR} = 160 nm, N_{DBR} = 400, d_{GC} = 874.4 nm, c_{GC} = 225 nm, N_{GC} = 21.

section 3 than for the structures of section 2, since the effective index of the modes in the GC and DBR is slightly nearer to that of the PS (n_G = 1.9963) for the structures of section 3 ($\tilde{n}$ = 1.771) than for structures of section 2 ($\tilde{n}$ = 1.759).

Table 3. Parameters of the CRIGF with an optimized bi-atom GC and DBR with impedance match[a]

Structure	δ	Δ_a	Δ_b
DBR1.25-IM	1.25	397.0	410.0
DBR2.5-IM	2.5	398.3	410.0
DBR5-IM	5	402.6	408.0
DBR10-IM	10	402.6	414.1

[a]All dimensions in nanometers. Common parameters: c = 100 nm, d_{DBR} = 437.2 nm, c_{DBR} = 160 nm, N_{DBR} = 400, d_{GC} = 874.4 nm, c_{GC} = 225 nm, N_{GC} = 21.

As already done in [16], we reduce this mismatch thanks to an additional groove with width c inside the two PS regions between the GC and the DBR (see Fig. 7).

Optics EXPRESS

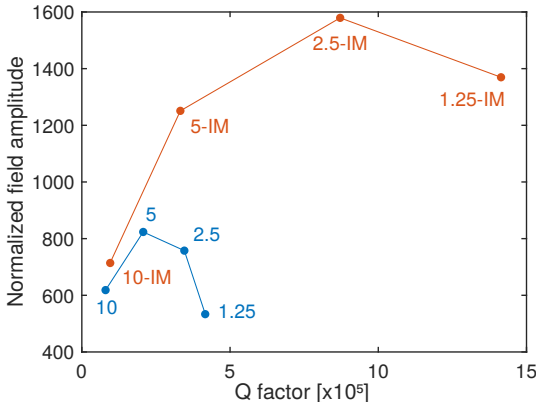

Fig. 6. Mode amplitude, normalized with respect to the square root of the incident power ($V.\mu m^{-1}.W^{-1/2}$), versus the Q-factor for the CRIGF of Table 2 (blue) and Table 3 (orange).

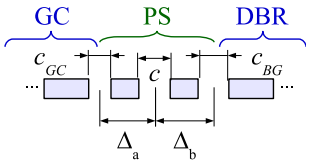

Fig. 7. Impedance matched CRIGFs (IM): an extra groove is added within the phase section *PS*. For each particular CRIGF, the width c and the distances Δ_a & Δ_b result from a numerical optimization.

The parameters c, Δ_a and Δ_b, used to tune the length of the phase shift region, are chosen to maximize the field amplitude, and are given in Table 3 (structures labelled DBR1.25-IM to DBR10-IM, where IM stands for impedance match).

The evolution of the field amplitude with respect to the Q-factor is reported in Fig. 6 (orange dots). We observe that even higher Q-factors and field amplitudes are obtained. The decrease of the field amplitude occurs for greater Q-factors than for the structures without reduced mode mismatch, leading to a huge mode enhancement for the DBR2.5-IM structure.

Finally, we calculate the SHG power emitted in the substrate and superstrate. Table 4 reports the conversion factor η for the eight structures of Table 2 and Table 3, sorted with decreasing η. As expected, the higher the field amplitude, the higher the conversion factor. Even greater conversion factors than for the structures of the previous section are demonstrated : $\eta = 0.647\,W^{-1}$, $0.370\,W^{-1}$ and $0.255\,W^{-1}$ respectively for structures DBR2.5-IM, DBR1.25-IM and DBR5-IM. These values are also greater than that obtained with the asymmetric structure and an additional groove within the PS region reported in [16] ($0.149\,W^{-1}$, for structure ASYM-IM).

We emphasize that these results are obtained without phase-matching between the mode at the pump and the mode at the signal frequency. In the next section, we explore, still using the same layer stack, the improvement that can be obtained thanks to an additional structure designed to ensure grating-assisted phase-matching.

Optics EXPRESS

Table 4. Conversion efficiency of the CRIGF with an optimized bi-atom GC and DBR with and without impedance match[a]

Structure	$\eta\ [W^{-1}]$
DBR2.5-IM	0.647
DBR1.25-IM	0.370
DBR5-IM	0.255
DBR5	0.0489
DBR2.5	0.0354
DBR10-IM	0.0270
DBR10	0.0151
DBR1.25	0.00874

[a](parameters in Table 2 and 3)

5. CRIGF with a bi-atom GC and grating phase-matching

It is well known that SHG is enhanced when the source/pump and the second harmonic wave are phase-matched. In bulk media and waveguides, the phase-matching condition requires that the effective index $\tilde{n}(\omega)$ at the pump frequency is equal to the effective index $\tilde{n}(2\omega)$ at the signal frequency. In bulk anisotropic material, one usually tune the angle of propagation to achieve phase-matching. In multimode waveguides with many layers, phase-matching can be achieved using a careful optimization of the multilayer stack. For few-layers monomode stack, it is possible to realize phase-matching thanks to a well-chosen grating, usually phase-matching counter-propagating pump and signal modes. The grating-assisted phase-matching can be done either at the signal or pump frequency, as explained below and as described in Fig. 8. For both, the starting point is the forward propagating eigenmode excited at the pump frequency (red disc in Fig. 8).

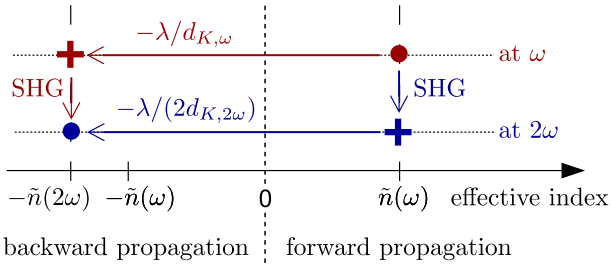

Fig. 8. Scheme of grating phase-matching at the pump frequency ω (in red) and at the signal frequency 2ω (in blue). The disc stand for the eigen-modes, while the crosses stand for non-resonant electromagnetic fields.

For a phase-matching at the signal frequency 2ω (corresponding to the signal wavelength $\lambda/2$), we consider: on the one hand *the field created at the signal frequency* by non-linear conversion from this eigenmode (blue cross on Fig. 8), and on the other hand *the backward propagating eigenmode at the signal frequency* (effective index $-\tilde{n}(2\omega)$, blue disc on Fig. 8). The spatial period of the field created at the signal frequency correspond to an effective index of $\tilde{n}(\omega)$. In order to couple this field to the counterpropagating eigen-mode, the period $d_{K,2\omega}$ of the grating

Optics EXPRESS

should satisfy the relation

$$\tilde{n}(\omega) + \tilde{n}(2\omega) = \frac{\lambda}{2d_{K,2\omega}}, \tag{7}$$

when the first diffraction order of the grating is used. This coupling is represented by the horizontal blue arrow on Fig. 8. We will call this 2ω-phase-matching. The improvement of SHG due to this kind of phase-matching for guided mode resonance waveguide has already been demonstrated in the literature [3].

Alternatively, for a phase-matching at the pump frequency ω (corresponding to the pump wavelength λ), we consider: on the one hand *the forward propagating eigen-mode at the pump frequency* (effective index $\tilde{n}(\omega)$, red disc on Fig. 8), and on the other hand, *the field at the pump frequency* ω that will generate by non-linear conversion a field at 2ω matching the backward propagating eigenmode at 2ω with effective index $-\tilde{n}(2\omega)$ (red cross on Fig. 8). The effective index of this latter field *at the pump frequency* is also $-\tilde{n}(2\omega)$. In this case, the period $d_{K,\omega}$ of the phase-matching grating must satisfy the relation

$$\tilde{n}(\omega) + \tilde{n}(2\omega) = \frac{\lambda}{d_{K,\omega}}. \tag{8}$$

This coupling is represented by the horizontal red arrow on Fig. 8. We will call this ω-phase-matching. The advantage is that the required period is twice as large as that of the 2ω-phase-matching, making the fabrication easier.

We consider the CRIGF of the previous section with GC parameters $c_{GC} = 225$ nm, $d_{GC} = 874.4$ nm and DBR parameters $c_{DBR} = 160$ nm, $d_{GC} = 437.2$ nm, and two values of δ, 2.5 nm and 5 nm. The effective index of the fundamental mode at the pump frequency is $\tilde{n}(\omega) \simeq 1.771$, and at the signal frequency $\tilde{n}(2\omega) \simeq 2.023$. Equations (7) and (8) are used to obtain a starting value for the period of the phase-matching grating.

Then further optimization steps are performed on the period and the filling factor of the phase-matching gratings so that the effective index of the mode within the phase-matching grating is close to that in the GC and DBR regions at λ_0. This leads to $d_{K,2\omega} = 204.4$ nm and $c_{K,2\omega} = 39.8$ nm for the 2ω-phase-matching, and $d_{K,\omega} = 408.5$ nm and $c_{K,\omega} = 68.1$ nm for the ω-phase-matching. The phase-matching grating K is added between the GC, after the phase section PS_1, and the DBR, before the phase section PS_2 (see Fig. 9). The number of periods of the phase-matching grating is chosen equal to $N_K = 300$ for the 2ω-phase-matching and $N_K = 160$ for the ω-phase-matching, in order to have comparable lengths of the two structures, despite the twice larger period for the ω-phase-matching grating. The PS_1 and PS_2 lengths are determined to maximize the pump field amplitude in the structure. The parameters of the four structures are gathered in Table 5.

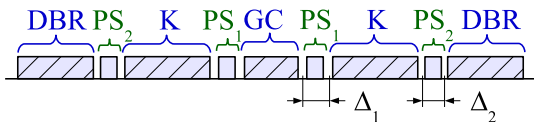

Fig. 9. Additional grating (K) for grating-assisted phase-matching, with N_K grooves with width c_K and period d_K (the grooves are not represented).

In order to verify that the desired modes are excited, we plot on Fig. 10 the field at resonance in the Fourier space, for structures DBR5-K_ω (blue line) and DBR5-$K_{2\omega}$ (orange line) at ω for Fig. 10 (a) and 2ω for Fig. 10 (b). At ω, as expected, the field is strong at an effective index close to that of the fundamental TE mode of the structure ($\tilde{n}(\omega) = 1.771$, peak 1), for both structures. For DBR5-K_ω we can see a second peak (peak 2), corresponding to an effective index close

Optics EXPRESS

Table 5. Parameters of the CRIGF with a grating phase-matching[a]

Structure	δ	N_K	d_K	c_K	Δ_1	Δ_2
DBR2.5-K_ω	2.5	160	408.5	68.1	425.0	508.5
DBR2.5-$K_{2\omega}$	2.5	300	204.4	39.8	137.8	440.0
DBR5-K_ω	5	160	408.5	68.1	443.5	489.5
DBR5-$K_{2\omega}$	5	301	204.4	39.8	300.0	407.4

[a]All dimensions in nanometers. Common parameters: d_{DBR} = 437.2 nm, c_{DBR} = 160 nm, N_{DBR} = 400, d_{GC} = 874.4 nm, c_{GC} = 225 nm, N_{GC} = 21.

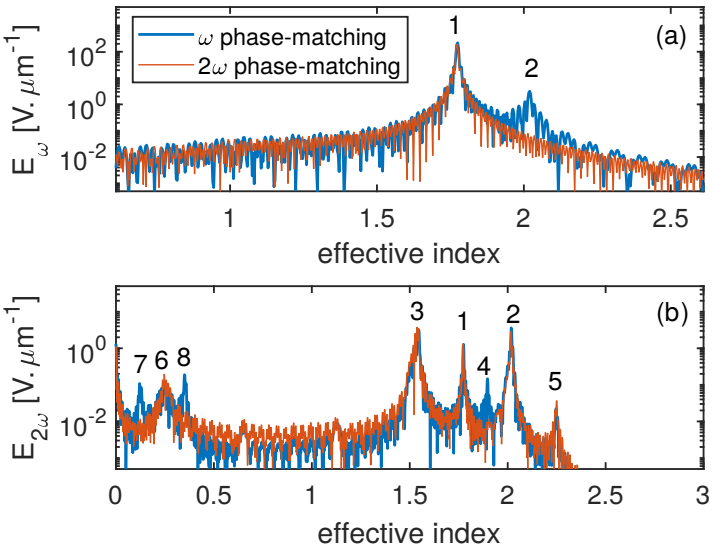

Fig. 10. Field at the bottom interface of the structure, at resonance, in the Fourier space for structures DBR5-K_ω (blue line) and DBR5-$K_{2\omega}$ (orange line) at ω (a) and 2ω (b).

to $\tilde{n}(2\omega) = 2.023$, obtained as desired from the fundamental TE mode thanks to the coupling through the first order of the phase-matching grating.

The field at 2ω (Fig. 10 (b)) is much more complicated. The peaks 1 and 2 are directly obtained by non-linear conversion from the peaks 1 and 2 existing at ω. The non-linear conversion of the ω-field also gives a strong peak centered at 0. Peak 3 corresponds to the second TE mode ($\tilde{n'}(2\omega) = 1.538$). Peak 4 comes from the coupling, through the +1 order of the grating $K_{2\omega}$ or +2 order of K_ω, of the negative counterpart of peak 3. Peak 5, somewhat large, has two contributions: the coupling through the −1 order of the DBR of peak 2, and the coupling through the +1 order of the DBR of the negative counterpart of peak 1. The coupling of peak 3 through the +/−1 order of the DBR gives peaks close to 0. Peaks 6 is similar to peak 5 except that it is obtained thanks to the K_ω grating, and peak 7 comes from the coupling of the negative counterpart of peak 3 through the +1 order of the K_ω grating. Last, peak 8 corresponds to the coupling, through the +1 diffraction order of the K_ω grating, of the peak centered at 0. It must be noted that peaks 5, 6 and 7 correspond to fields coupled-out in the substrate and superstrate. Hence, we can expect a conversion efficiency slightly greater for structure DBR5-K_ω than for DBR5-$K_{2\omega}$. Similar features are obtained with structures DBR2.5-K_ω and DBR2.5-$K_{2\omega}$.

Optics EXPRESS

The conversion efficiency factors obtained for the four grating-assisted phase-matched structures are gathered in Table 6, where the conversion efficiencies for the two impedance-matched structures with $\delta = 2.5$ nm and $\delta = 5$ nm are also presented for comparison.

Table 6. Conversion efficiencies for the ω and 2ω-phase-matched, and impedance-matched structures.

Structure	$\eta\ [W^{-1}]$	Structure	$\eta\ [W^{-1}]$
DBR2.5-IM	0.647	DBR5-IM	0.255
DBR2.5-K$_\omega$	1.556	DBR5-K$_\omega$	0.643
DBR2.5-K$_{2\omega}$	1.379	DBR5-K$_{2\omega}$	0.601

We observe that using a ω-phase-matching grating gives slightly greater conversion efficiencies than with a 2ω-phase-matching, as can be expected from the field at resonance in the Fourier space (Fig. 10 (b)). Higher conversion efficiencies are obtained for smaller δ, due to the highest Q-factor. Last, the comparison with respect to structures DBR2.5-IM and DBR5-IM shows greater conversion efficiency for the grating-assisted phase-matching structures. About 70 % of this improvement is due to the longer cavity in the grating-assisted phase-matching structures.

6. Conclusion

We numerically demonstrated high SHG conversion efficiencies using cavity-resonator integrated grating couplers with a bi-atom GC base pattern. This particular pattern is close to the pattern of the surrounding distributed Bragg reflectors and is not particularly challenging to fabricate. We worked on a simple stack, composed from a dielectric grating on the non-linear material layer, without aiming at direct phase-matching between a mode at the pump frequency and a mode at the signal frequency. We explained the main design rules, necessary to match the effective index of the modes within the GC section and DBR section, while keeping an efficient DBR and a high Q-factor GC. We showed one order of magnitude improvement of the SHG conversion efficiency η with respect to our previous publication relying on asymmetric structures [16]. Cutting the PS into two parts decreases the scattering losses at the transitions between the GC, the PS and the DBR, and leads to η greater than 0.1 W^{-1} (impedance-matched structures). Finally, we explored the benefit of introducing a grating phase-matching, either at the pump or signal frequency, which doubles the conversion efficiency of the impedance-matched structure. This work demonstrates how CRIGFs can achieve conversion factors of the same order of magnitude as waveguides or nano-resonators.

Funding. Direction Générale de l'Armement (ANR-19-ASTR-0019).

Acknowledgments. This work was supported by French Defense Innovation Agency (AID) under grant ASTRID RESON ANR-19-ASTR-0019.

Disclosures. Authors declare no conflict of interest.

Data availability. Data underlying the results presented in this paper are not publicly available at this time but may be obtained from the authors upon reasonable request.

References

1. F. Renaud, A. Monmayrant, S. Calvez, O. Gauthier-Lafaye, A.-L. Fehrembach, and E. Popov, "Second-harmonic-generation enhancement in cavity resonator integrated grating filters," Opt. Lett. **44**(21), 5198–5201 (2019).
2. A. Cowan and J. Young, "Mode matching for second-harmonic generation in photonic crystal waveguides," Phys. Rev. B **65**(8), 085106 (2002).
3. G. Blau, E. Popov, F. Kajzar, A. Raimond, J.-L. Roux, and J.-L. Coutaz, "Grating-assisted phase-matched second-harmonic generation from a polymer waveguide," Opt. Lett. **20**(10), 1101–1103 (1995).
4. M. Siltanen, S. Leivo, P. Voima, M. Kauranen, P. Karvinen, P. Vahimaa, and M. Kuittinen, "Strong enhancement of second-harmonic generation in all-dielectric resonant waveguide grating," Appl. Phys. Lett. **91**(11), 111109 (2007).

Optics EXPRESS

5. G. Poberaj, H. Hu, W. Sohler, and P. Gunter, "Lithium niobate on insulator (LNOI) for micro-photonic devices," Laser Photonics Rev. **6**(4), 488–503 (2012).
6. C. Wang, K. Zhaoyi, L. Myoung-Hwan, X. Xiong, X.-F. Ren, G.-C. Guo, N. Yu, and M. Loncar, "Metasurface-assisted phase-matching-free secondharmonic generation in lithium niobate waveguides," Nat. Commun. **8**(1), 2098 (2017).
7. C. Wang, X. Xiong, N. Andrade, V. Venkataraman, X.-F. Ren, G.-C. Guo, and M. Loncar, "Second harmonic generation in nano-structured thin-filmlithium niobate waveguides," Opt. Express **25**(6), 6963–6973 (2017).
8. M. Borghi, C. Castellan, S. Signorini, A. Trenti, and L. Pavesi, "Nonlinear silicon photonics," J. Opt. **19**(9), 093002 (2017).
9. A. Boes, B. Corcoran, L. Chang, J. Bowers, and A. Mitchell, "Status and potential of lithium niobate on insulator (LNOI) for photonic integrated circuits," Laser Photonics Rev. **12**(4), 1700256 (2018).
10. J. Bravo-Abad, S. Fan, S. Johnson, J. Joannopoulos, and M. Soljacic, "Modeling nonlinear optical phenomena in nanophotonics," J. Lightwave Technol. **25**(9), 2539–2546 (2007).
11. N. Segal, S. Keren-Zur, N. Hendler, and T. Ellenbogen, "Controlling light with metamaterial-based nonlinear photonic crystals," Nat. Photonics **9**(3), 180–184 (2015).
12. M. Logan, A. Gould, E. Shmidgall, K. Hestroffer, Z. Lin, A. Jin, W. Majumdar, F. Hatami, A. Rodriguez, and K.-M. Fu, "400 percent/W second harmonic conversion efficiency in 14micrometer-diameter gallium phosphide-o-oxide resonators," Opt. Express **26**(26), 33687 (2018).
13. A. Krasnok, M. Tymchenko, and A. Alu, "Nonlinear metasurfaces: A paradigm shift in nonlinear optics," Mater. Today **21**(1), 8–21 (2018).
14. R. Mohsen, G. Leo, I. Brener, A. V. Zayats, S. A. Maier, C. De Angelis, and H. e. a. Tan, "Nonlinear frequency conversion in optical nanoantennas and metasurfaces: Materials evolution and fabrication," Opto-Electron. Adv. **1**(10), 18002101 (2018).
15. A.-L. Fehrembach, B. Gralak, and A. Sentenac, "Vectorial model for guided-mode resonance gratings," Phys. Rev. A **97**(4), 043852 (2018).
16. A.-L. Fehrembach, F. Renaud, E. Popov, H. Tortel, A. Monmayrant, O. Gauthier-Lafaye, and S. Calvez, "Dark mode-in-the-box for enhanced second-harmonic generation in corrugated waveguides," Opt. Express **29**(25), 40981 (2021).
17. F. Lemarchand, A. Sentenac, and H. Giovannini, "Increasing the angular tolerance of resonant grating filters with doubly periodic structures," Opt. Lett. **23**(15), 1149–1151 (1998).
18. T. Ning, X. Li, Y. Zhao, L. Yin, Y. Huo, L. Zhao, and Q. Yue, "Giant enhancement of harmonic generation in all-dielectric resonant waveguide gratings of quasi-bound states in the continuum," Opt. Express **28**(23), 34024–34034 (2020).
19. R. Laberdesque, O. Gauthier-Lafaye, H. Camon, A. Monmayrant, M. Petit, O. Demichel, and B. Cluzel, "High-order modes in cavity-resonator-integrated guided-mode resonance filters (CRIGFs)," J. Opt. Soc. Am. A **32**(11), 1973–1981 (2015).
20. N. Rassem, A.-L. Fehrembach, and E. Popov, "Waveguide mode in the box with an extraordinary flat dispersion curve," J. Opt. Soc. Am. A **32**(3), 420–430 (2015).
21. F. Renaud, G. Mohamed, A.-L. Fehrembach, E. Popov, A. Monmayrant, and O. Gauthier-Lafaye, "Quasi-total backward reflection with a CRIGF under oblique incidence," Opt. Quantum Electron. **52**(3), 184 (2020).
22. P. Chaumet, G. Demésy, O. Gauthier-Lafaye, A. Sentenac, E. Popov, and A.-L. Fehrembach, "Electromagnetic modeling of large subwavelength-patterned highly resonant structures," Opt. Lett. **41**(10), 2358–2361 (2016).
23. W. Nakagawa, T. Rong-Chung, and Y. Fainman, "Analysis of enhanced second-harmonic generation in periodic nanostructures using modified rigorous coupled-wave analysis in the undepleted-pump approximation," J. Opt. Soc. Am. A **19**(9), 1919–1928 (2002).
24. B. Bai and J. Turunen, "Fourier modal method for the analysis of second-harmonic generation in two-dimensionally periodic structures containing anisotropic materials," J. Opt. Soc. Am. B **24**(5), 1105–1112 (2007).
25. A. Yariv, "Universal relationsfor coupling of opticalpower between microresonatorsanddielectric waveguides," Electron. Lett. **36**(4), 321–322 (2000).
26. Y. Dumeige, S. Trebaol, L. Ghişa, T. K. N. Nguyên, H. Tavernier, and P. Féron, "Determination of coupling regime of high-Q resonators and optical gain of highly selective amplifiers," J. Opt. Soc. Am. B **25**(12), 2073–2080 (2008).
27. E. Popov, E. Hemsley, A.-L. Fehrembach, O. Gauthier-Lafaye, A. Monmayrant, and S. Calvez, "Extreme enhancement of the quality (Q)-factor and mode field intensity in cavity-resonator gratings," Opt. Express **30**(14), 25390 (2022).